PERGAMON

International Journal of Solids and Structures 36 (1999) 2259–2283

INTERNATIONAL JOURNAL OF SOLIDS and STRUCTURES

Numerical analysis of cracked inelastic shells with large displacements or mixed mode loading

Bjørn Skallerud*

Division of Applied Mechanics, The Norwegian University of Science and Technology, N-7034, Trondheim, Norway[1]

Received 24 June 1997; in revised form 8 March 1998

Abstract

The trend in higher utilization of structural materials leads to a need for accurate numerical tools for reliable predictions of structural response. In some instances both material and geometrical nonlinearities are allowed for, typically in assessments of structural collapse or residual strength in damaged conditions. Dynamically loaded structures are prone to fatigue cracking; this has to be accounted for when computing nonlinear structural response. The present study addresses the performance of cracked inelastic shells with out-of-plane displacement not negligible compared to shell thickness. This situation leads to membrane force effects in the shell. Hence, a cracked part of the shell will be subjected to a nonproportional history of bending moment and membrane force, and e.g. fracture mechanics parameters (J-integral) are affected. A Mindlin shell finite element based nonlinear program is developed and utilized herein. The cracked parts are accounted for by means of inelastic line spring elements. These elements also account for possible mode II deformations.

1. Introduction

The numerical analysis of shell type of structures by means of finite elements, accounting for geometrical and material nonlinearity, has developed significantly during the last decades. A summary of recent advances is given by Crisfield (1997). Due to the strong nonlinear behaviour in shell instability problems, much research on developing robust methods for solution of the evolution of global equilibrium equations in an incremental-iterative setting has successfully been carried out. Although still not trivial, one now has algorithms that handle limit points and snap back/snap through problems. Robust methods for updating stresses at integration points have also been developed, e.g. backward Euler integration of the elastic–plastic problem along with the

* Fax: 0047 73 59 34 91. e-mail: bjoern.skallerud@ntf.ntne.no

[1] Work partially carried out during a stay at Dep. Building Tech. and Struct. Engng, University of Aalborg, Denmark.

0020–7683/99/$ - see front matter
PII: S0020–7683(98)00110–3

consistent linearisation of the updating in order to preserve the asymptotically quadratic rate of convergence in the Newton–Raphson iteration on the global equilibrium equations. Furthermore, much effort has been put in deriving shell finite elements that account for out-of-plane shear deformations in thick shells that are free of locking problems in the thin shell limit. All problems regarding nonlinear shell behaviour have still not been solved, however, and due to the extensive use of shell type of structures (pressure vessels, pipelines, offshore platforms) still this is an active research area. Shells subjected to variable loading (dynamically or quasi-statically) may develop cracks, this is especially the case for shells with attachments such as stiffeners or other out-of-plane components welded to the shell. Usually the material applied in the shell structures mentioned above is very ductile. As a consequence, the cracked shell allows (significant) inelastic deformations without/before fracturing. In order to check the capacity, nonlinear fracture mechanics may be utilised, typically by means of calculation of the *J*-integral (Rice, 1968) or the crack tip opening displacement CTOD (Cottrell, 1961; Wells, 1961), and compare these quantities against the corresponding critical quantities. According to recent research these fracture criteria should be supplemented with a parameter measuring the constraint in the crack tip region. A methodology based on T-stress or Q-parameter is under development (Betegon and Hancock, 1991; O'Dowd and Shih, 1992; Parks, 1992; Kirk and Bakker, 1995). Although it is possible to do non-linear solid finite element analysis of cracked shell structures in order to compute the fracture mechanics quantities, or even calculate the damage evolution from fracture initiation to failure by means of damage mechanics, the size of these problems in relation to computer resources often precludes such analyses to be carried out. An alternative way of solving these problems is the combination of shell and line spring finite elements (Rice and Levy, 1972; Parks and White, 1982). Now the 3-D problem is simplified to a 2-D one, with solution of equation systems of size one order of magnitude lower than in the 3-D case. Such analyses may effectively be carried out today. The accuracy in computed response and fracture mechanical parameters by this method is satisfactory for engineering applications. Over the last decade there has been development of the line spring modelling, e.g. accounting for a crack tip plastic zone that leads to line spring response (load vs deformation) appearing softer in the transition between elastic and plastic regime as if the actual crack was slightly larger (Lee and Parks, 1995); improved Mode I yield surfaces for the fully plastic performance of the line spring for larger range of crack depth to shell thickness ratios (Lee and Parks, 1993), mixed mode I/II yield surfaces (Skallerud, 1996), ductile tearing line spring (Lee and Parks, 1997). To the author's knowledge, a point that still has not been considered is the effect of large out-of-plane displacements on the response of cracked shells. Such displacements may occur in components that have out-of-plane load carrying attachments. An important relevant case in this respect is illustrated in Fig. 1 (Skallerud, 1995). Here a tubular joint transfers the brace loading into the chord. If the brace load exceeds the levels where the global response is linear, the chord may change shape as illustrated in Fig. 1(b), i.e. a nonlinear geometrical effect. Figure 1(c) further details the joint in the brace-chord transition, illustrating the weld by the hatched region. The weld toe is prone to fatigue crack growth, and in an overload situation this part of the shell may be subjected to both material and geometrical nonlinearities. Note also that the cracked chord region is subjected to both mode I and mode II loading.

The present investigation addresses situations such as depicted in Fig. 1(b), i.e. shells with significant loading out-of-plane. In order to simplify the problem, the main geometries studied are cracked flat shells, accounting for plasticity and membrane stresses developing due to the finite

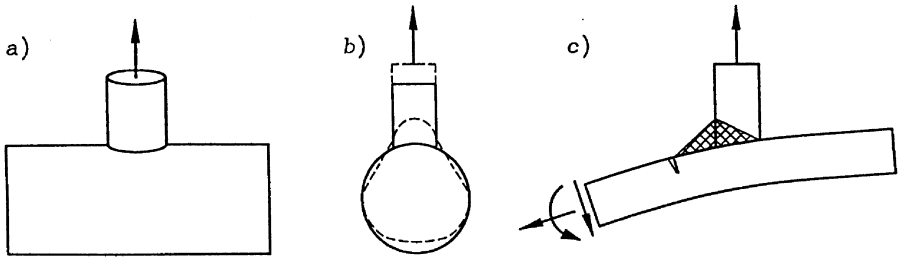

Fig. 1. Large deformation in cracked tubular joint.

out-of-plane displacements. In the first part of the study, the cracked plate is simplified to rigid plates connected with inelastic line springs. Hence, the governing deformations are due to the elastic-plastic deformations in the crack region ligament. For shell structures with large-width surface cracks this is representative. This part also presents the basic line spring relationships. In the second part, the line spring is utilised in a nonlinear shell finite element program developed within the course of the study, called SHEL*ls*. Here plates/shells with semi-elliptical cracks are studied.

2. Rigid plate—line spring geometries

Figure 2(a) shows the plan view of a cracked plate loaded out-of-plane. The plate width (normal to figure) is assumed large, hence having a plane strain situation. Taking the two plate parts as rigid, the deformations are accounted for by the line spring as illustrated in Fig. 2(b). During load application the vertical deflection leads to a rotation. If the boundary conditions at each end of the plate is fixed with respect to in plane displacements, axial deformation of the line spring develops due to this restraint. The vertical spring accounts for eventual Mode II deformations. For the case in Fig. 2(b) no Mode II is present, but placing the crack eccentrically as shown in Fig. 2(c), this deformation occurs. It should be noted that the line spring stiffness refers to the mid-thickness of the plate. The gap between the two rigid plates in Fig. 2(b) is for illustration purposes, the length of the rigid plates is taken as l subsequently, hence the springs have vanishing extension in length direction before loading. Finally, as long as the line spring is elastic there is connection between axial and bending deformation and no connection with the shear deformation. Inelastically, however, all deformation modes may interact.

2.1. The mixed mode I/II line spring model

For completeness some of the line spring relationships are presented here. Further details may be found in (Rice and Levy, 1972; Parks and White, 1982; Skallerud, 1996). The line spring simulates the additional flexibility of a shell due to a cracked part. Figure 3(a–c) illustrate the main features for Mode I loading, from the basic plane strain model where $a/c = 0$ ($c = \infty$ is the crack size in x-direction), via using the crack depth at a given x co-ordinate for semi-elliptical cracks as

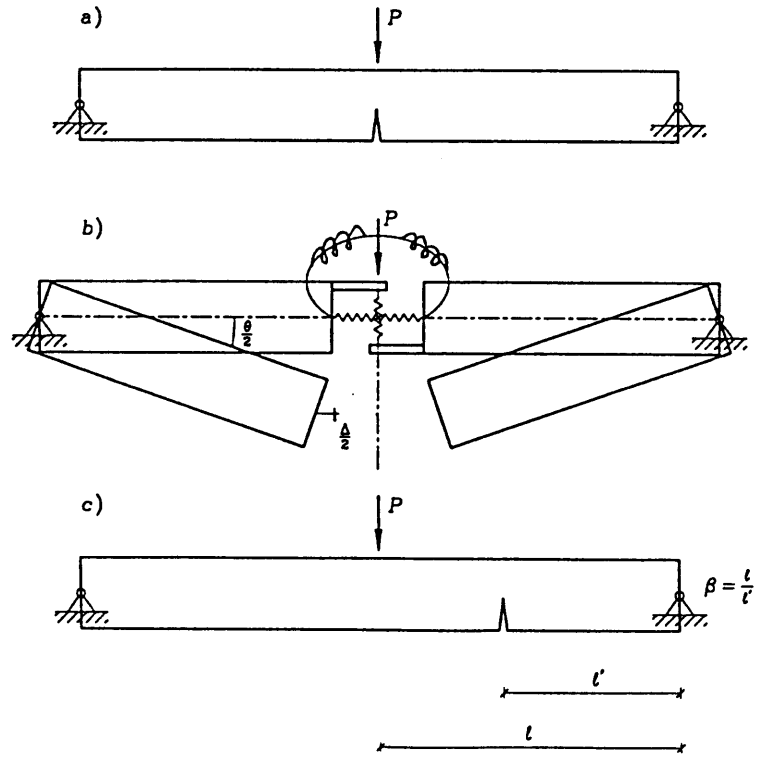

Fig. 2. Rigid plate inelastic line spring.

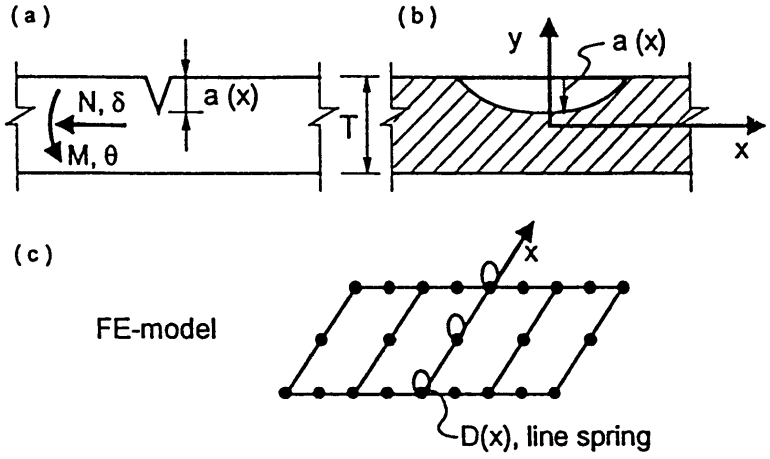

Fig. 3. Line spring concepts.

input to determine the flexibility at that co-ordinate, to discretized line spring stiffnesses in a shell finite element model.

The connection between the line spring deformations and energy conjugate forces in the elastic regime is expressed as:

$$\Delta = C_{NN}N + C_{NM}M$$
$$\theta = C_{MN}N + C_{MM}M$$
$$\xi = C_{VV}V$$
$$C_{NM} = C_{MN}$$
$$\mathbf{q} = \mathbf{C}_e\mathbf{Q} \tag{1}$$

The compliances C_{ij} are obtained from known solutions for surface cracked strips (Rice and Levy, 1972). Inverting the compliance matrix yields the elastic stiffness matrix for the cracked section:

$$\mathbf{Q} = \mathbf{D}_e\mathbf{q} = \mathbf{C}_e^{-1}\mathbf{q} \tag{2}$$

The mixed mode I/II lower bound yield surface employed in (Skallerud, 1996) reads:

$$f(N, M, V, \sigma_y; c) = \left[\frac{N}{N_p}\right]^2 + \left[\frac{M + N(t-c)0.5}{M_p}\right] + \left[\frac{V}{V_p}\right]^2 - 1$$

$$N_p = \sigma_y c, \quad M_p = \tfrac{1}{4}\sigma_y c^2, \quad V_p = \frac{\sigma_y}{\sqrt{3}}c \tag{3}$$

Here, c is the ligament of the cracked section. One advantage with this relationship is, in addition to accounting for the transversal shear force, that the uncracked limit is obtained appropriately in contrast to upper bound solutions based on slip lines. The modification in uniaxial yield stress due to plane strain (multiplying with 1.15) is straightforward with this relationship, but for deep cracks (a/t approximately larger than 0.25) the crack increases the notional yield stress further by a factor 1.26 in predominant bending (Green and Hundy, 1956). As in (Skallerud, 1996), these factors are employed herein for $a/T \geqslant 0.25$. This reference may be conferred for further discussion and presentation of the lower bound yield surfaces. The lower bound yield surface [eqn (3)] is representative for tension and bending in the line spring. As shown in Fig. 4, for compression this yield surface is very non-conservative. Hence, for compression loading The modified Green–Hundy yield surface (White *et al.*, 1983) is employed. Lee and Parks (1993) have shown that for such loadings this surface is quite accurate. Subsequently, if the line spring axial force goes from compressive to tensile (as membrane effects develop), the yield surface applied is switched from the modified Green–Hundy solution to the lower bound solution.

Utilizing an additive decomposition of elastic and plastic line spring deformation increments, associated flow rule, plastic consistency, and an isotropic hardening rule, one establishes the tangent stiffness for the line spring:

$$\mathrm{d}\mathbf{q} = \mathrm{d}\mathbf{q}_e + \mathrm{d}\mathbf{q}_p$$
$$\mathrm{d}\mathbf{q}_p = \mathrm{d}q\frac{\partial f}{\partial \mathbf{Q}}$$

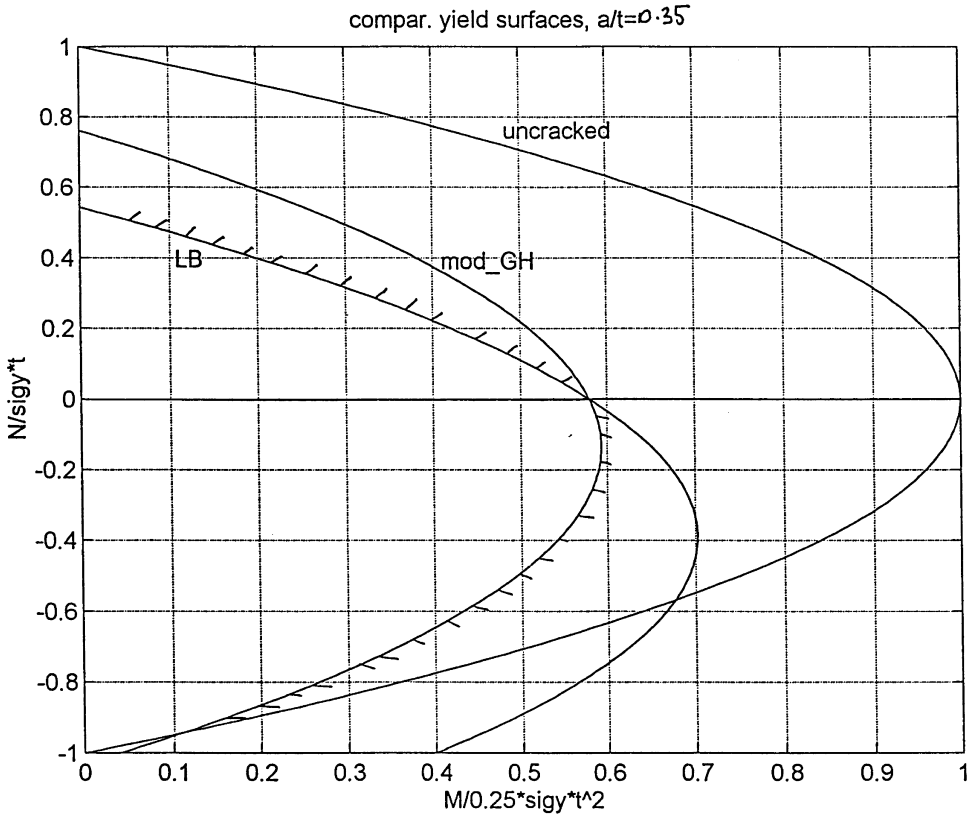

Fig. 4. Upper and lower bound yield surfaces.

$$\mathrm{d}f = \frac{\partial f^T}{\partial \mathbf{Q}}\mathrm{d}\mathbf{Q} + \frac{\partial f}{\partial \sigma_y}\mathrm{d}\sigma_y = 0$$

$$\mathrm{d}\mathbf{Q} = \left[\mathbf{D}_e - \frac{\left(\frac{\partial f^T}{\partial \mathbf{Q}}\mathbf{D}_e\right)^T \left(\frac{\partial f^T}{\partial \mathbf{Q}}\mathbf{D}_e\right)}{\frac{\partial f^T}{\partial \mathbf{Q}}\mathbf{D}_e\frac{\partial f}{\partial \mathbf{Q}} - \frac{\partial f^T}{\partial \mathbf{Q}}\mathbf{Q}\frac{\partial f}{\partial \sigma_y}\frac{E_p}{\sigma_y k c^{n'}}} \right] \mathrm{d}\mathbf{q} \tag{4}$$

The hardening rule is obtained by the argument that the plastic work increment of the stress resultants is equal to the continuum work increment integrated over the plastified ligament:

$$\mathrm{d}W_p = \mathbf{Q}^T \mathrm{d}\mathbf{q}_p = \int_{A_{\text{plastic}}} \sigma_{eq}\,\mathrm{d}\varepsilon_{p,eq}\,\mathrm{d}A = k\sigma_y \frac{\mathrm{d}\sigma_y}{E_p} c^{n'} \tag{5}$$

$$\mathrm{d}\varepsilon_p = \frac{\mathrm{d}\sigma_y}{E_p} \tag{6}$$

It has been shown that the continuum work is proportional to the averaged yield stress over the ligament multiplied by some plastically deforming area governed by ligament size c. Parks and White (1982) introduce a proportionality factor, denoted k in eqn (5). As found earlier, $k = 0.2$ and $n' = 2$ work well for the formulation above, and are employed herein also.

The elastic part of the mixed mode J may be determined directly from the current load level:

$$J_e = \frac{K_{\mathrm{I}}^2}{E'} + \frac{K_{\mathrm{II}}^2}{E'} \tag{7}$$

The mode I plastic J increment may be obtained from the plastic crack tip opening displacement, and this displacement is related to the line spring deformations by means of slip line kinematics:

$$\mathrm{d}J_{\mathrm{I},p} = m\sigma_y \,\mathrm{d}\delta_{\mathrm{I,cracktip},p} \tag{8}$$

$$\mathrm{d}\delta_{\mathrm{I,cracktip},p} = \mathrm{d}\Delta_p + \left(\frac{t}{2} - a\right)\mathrm{d}\theta_p \tag{9}$$

$$m = 1 + (M'/M_p)^3 \tag{10}$$

The above simple relationship for the constraint factor m has been discussed previously (Skallerud, 1996). Although rather crude, it simulates the variable constraint for the crack tip plastic zone for varying ligament tension/bending reasonably under the assumption that the crack tip stress field is governed by J. In mixed mode loading the following simple determination of plastic J-increment is assumed (Skallerud, 1996):

$$\mathrm{d}J_p = \mathrm{d}J_{\mathrm{I},p} + \mathrm{d}J_{\mathrm{II},p} = m\sigma_y\left[\mathrm{d}\Delta_p + \left(\frac{t}{2} - a\right)\mathrm{d}\theta_p\right] + m\frac{\sigma_y}{\sqrt{3}}\mathrm{d}\xi_p \tag{11}$$

2.2. Large displacement analysis of a centrally cracked, rigid plate

The situation analysed in this section is illustrated in Fig. 2(a) and (b). However, in order to circumvent the initial, artificially large compressive forces that develop in the line spring when the axial displacements at the boundaries are prevented at the mid-thickness of the plate, the boundaries are applied at the level of crack section *mid-ligament*. Otherwise, the problem would also include a snap-through behaviour before the ligament enters tension loading. Using a co-ordinate system based on the mid-ligament reference level, the elastic line spring stiffness is transformed accordingly by $\mathbf{T}^{\mathrm{T}}\mathbf{D}_{\mathrm{e}}\mathbf{T}$, where $\mathbf{T} = (1, -0.5a, 0; 0, 1, 0; 0, 0, 1)$ (the matrix rows are separated by semi-colons). The elastic–plastic results so obtained may now be compared to the analytic solution of the rigid plastic solution of a beam with a plastic hinge at midsection account for membrane force, extended to plane strain in order to simulate a wide plate:

$$P/P_0 = 1 + 4(v/t)^2, \quad v/t < 0.5$$
$$P/P_0 = 4(v/t), \quad v/t > 0.5 \tag{12}$$

Here P_0 is the plastic capacity due to bending alone. For the cracked plates the thickness t is replaced by the ligament c in the above equations. v is the transversal displacement.

The incremental connection between v and the line spring extension and rotation is

$d\Delta/2 = (v/l\sqrt{1+(v/l)^2})\,dv$ and $d\theta/2 = dv/l$, respectively. With this, terms of order higher than two is neglected. The incremental equilibrium of one half of the plate-spring system in the deformed configuration is $dP/2 \cdot l = dN \cdot v + N \cdot dv + dM$. Utilizing the tangent stiffness for the line spring and the connection between the line spring deformation and transversal displacement, a scalar equation for evolution of transversal load vs displacement is obtained.

Figure 5(a) shows the load vs displacement behaviour for the geometry in Fig. 2(a) keeping the plate half-length to ligament ratio constant equal to 50. The line spring material is assumed elastic–perfectly plastic. Three different a/t ratios are examined. When the curves get linear a situation of pure axial load in the line spring has developed. For $a/t = 0.25$ this occurs rapidly, for the plot of $a/t = 0.75$ this situation has not occurred for the level of displacement plotted. According to the rigid plastic analytic solution above, the pure membrane situation is reached for $v/c = 0.5$. From Fig. 5(a) one observes that for the two largest cracks this is delayed due to the elasticity of the line spring. For the smallest crack the behaviour resembles the analytic solution. For $a/t = 0.5$ the results are plotted again in Fig. 5(b) along with the rigid plastic solution eqn (12). One observes that the line spring result merges with the analytic solution when the displacement has reached a certain level. Note that the load–displacement curves would be horizontal after reached P_0 if the system only carried load by bending moment (i.e. horizontally free motion of the boundary displacement).

Figure 5(c) depicts the corresponding evolution of the J-integral for the three crack depths. The three upper curves represent the total J, the three lower represent the part of the J-integral caused by the second order membrane force in the line spring. This membrane contribution would be zero for a horizontally unrestrained boundary. The change in curvature of e.g. the $a/t = 0.5$ curve for large v/c is explained by Fig. 5(d). Here the evolution of the constraint factor is plotted, showing that initially it is two (bending dominated), then as the line spring carries more and more by membrane action, it approaches one. This leads to a corresponding reduction in the increase of the J-integral.

Figure 5(c) points out that if a transversally loaded cracked plate has in-plane restraints, and the loading is in displacement control, the J-integral will be under-estimated if the analysis assumes the load carrying by plate bending only. This observation is valid for large-width cracks, as other effects occur for finite widths, and is discussed in the second part. Additional analyses for other L/c-ratios show similar features as those given by Fig. 5.

2.3. *Analysis of an eccentrically cracked, welded T-connection*

In order to investigate a situation with both Mode I and II the specimen illustrated in Fig. 6(a) was analysed. At one weld toe a 7 mm deep surface crack was initiated by fatigue (note that all of the crack had this depth), and then the specimen was tested with respect to ductile fracture (Rabben, 1995). At each end of the horizontal plate, roller bearings were employed, i.e. unrestrained horizontally. The transversal load was applied in the vertical plate. The strains in y-direction were measured and compared with the corresponding strains in x-direction. These results showed that a plane strain situation was representative for the plates. Additionally, the specimen was analysed by means of detailed plane strain elementation with ABAQUS (Hibbitt *et al.*, 1993; Rabben, 1995), accounting for large deformations and damage growth. The details of these analyses will be presented elsewhere (Skallerud *et al.*, 1997). However some of the results are utilized herein for

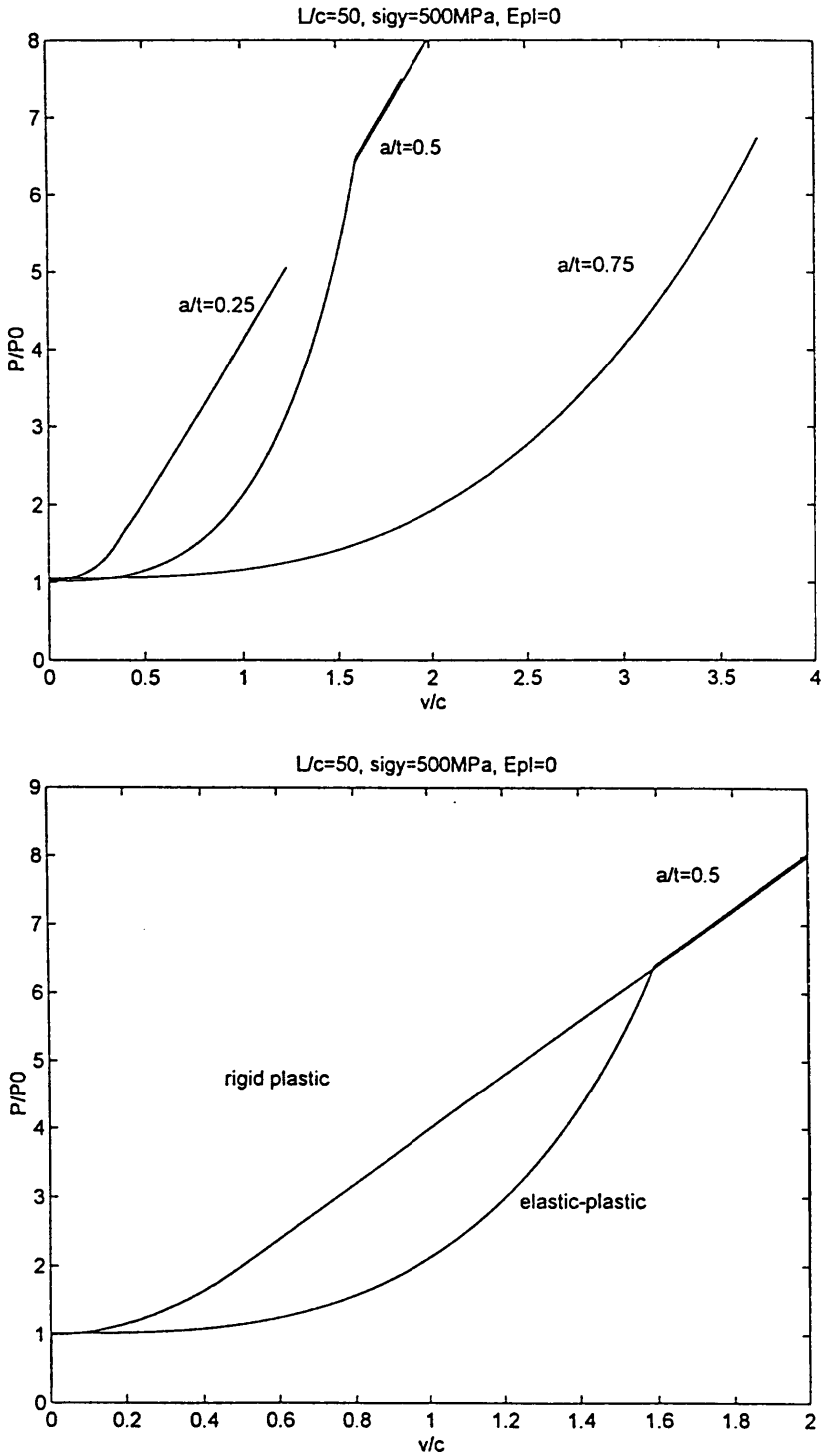

Fig. 5. (a) and (b) load vs displacement, (c) evolution of plastic J-integral, (d) evolution of constraint factor.

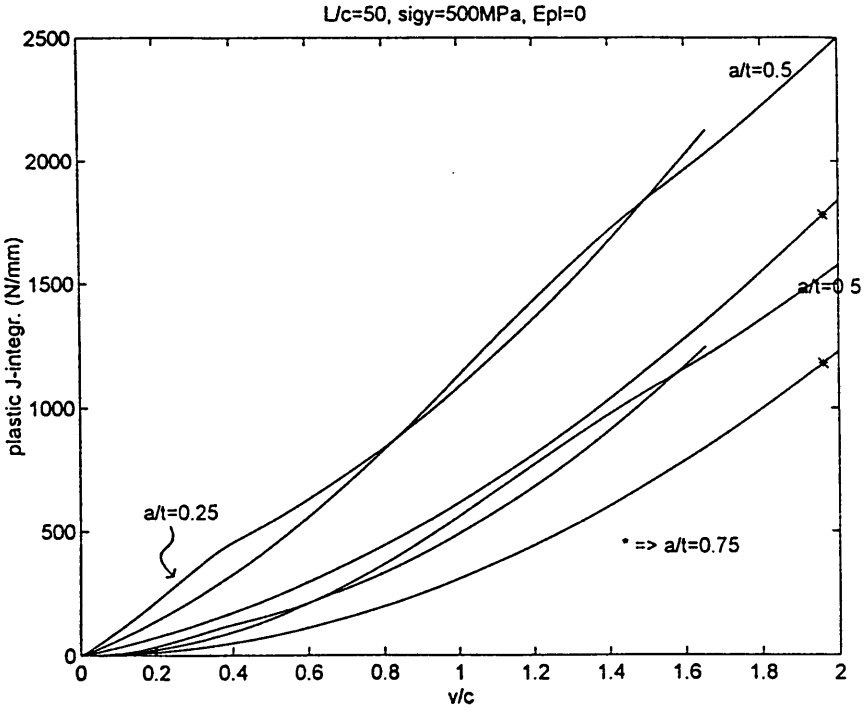

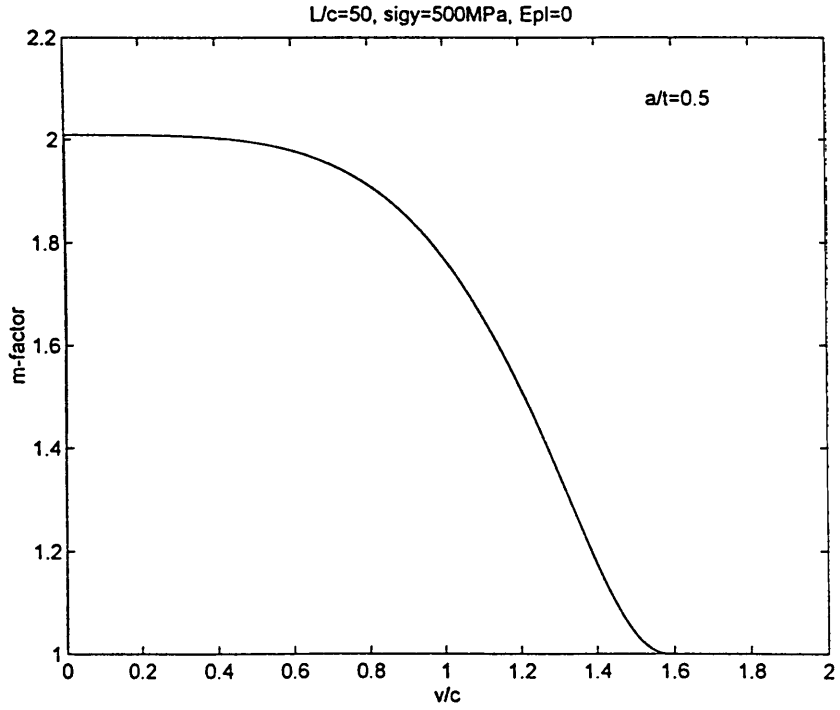

Fig. 5—*Continued.*

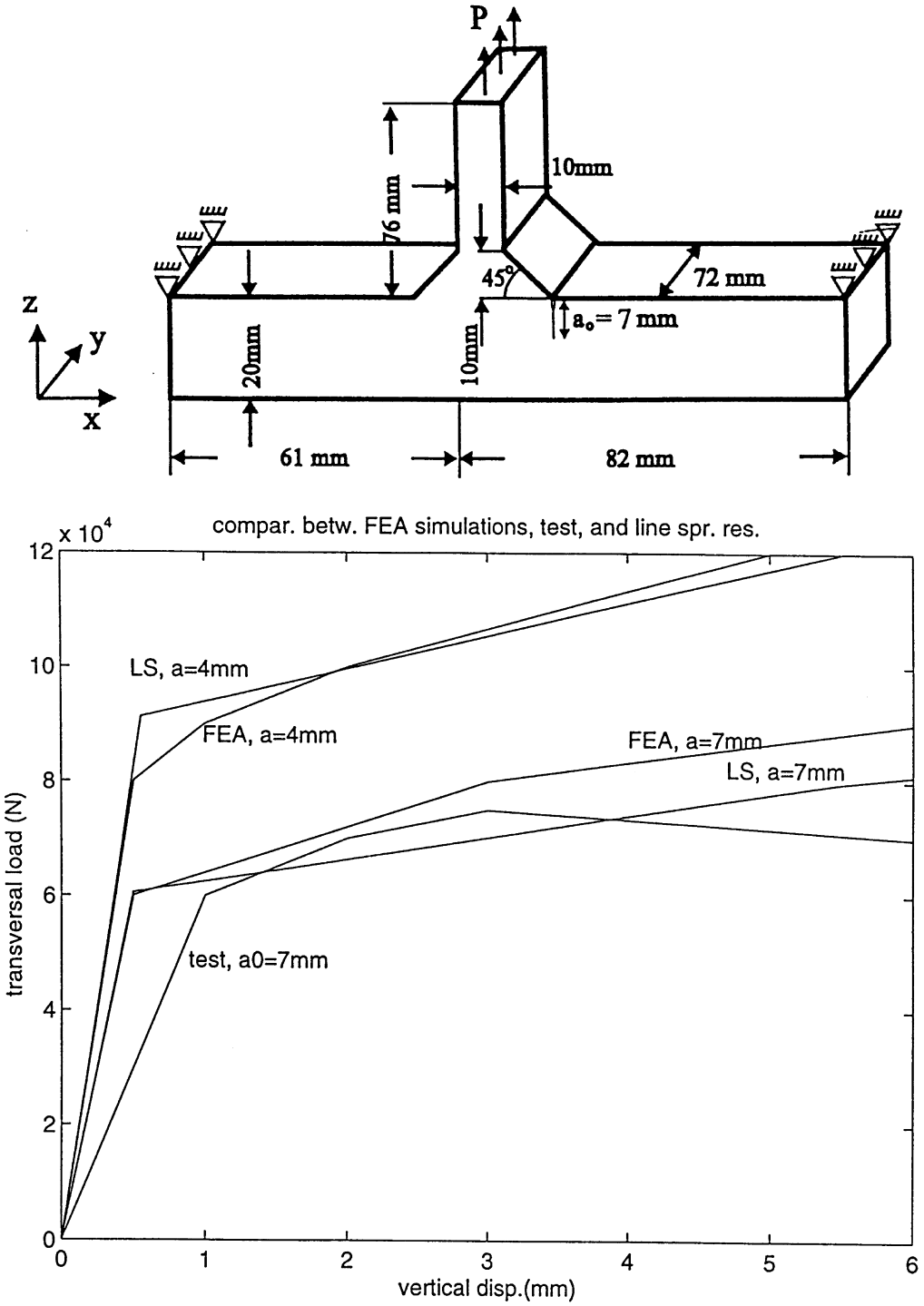

Fig. 6. (a) T-connection, (b) load vs displacement, (c) J-integral evolution.

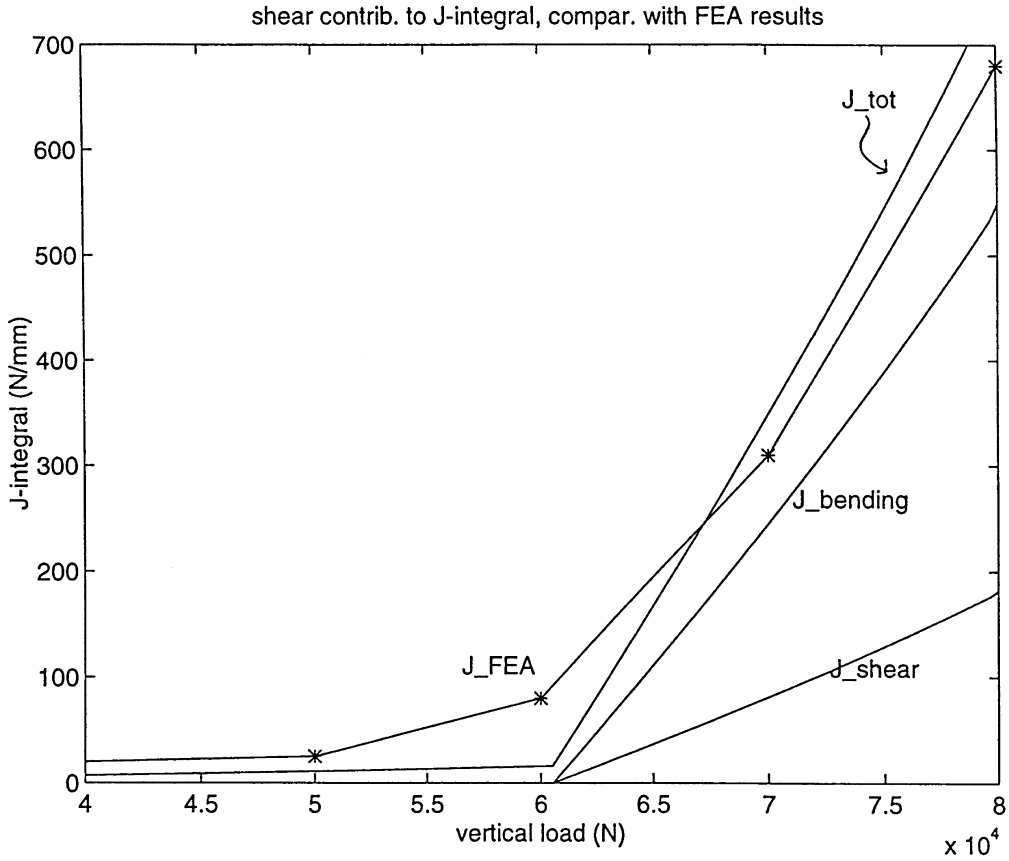

Fig. 6—*Continued.*

comparison with line spring analysis. The horizontal plate was assumed rigid in the line spring approach, and the static system was taken as shown in Fig. 2(c). The boundary is free to move horizontally, hence, the system carries load by bending and shear forces.

Figure 6(b) shows transversal load vs load line displacement for the T-connection. The curve denoted FEA is based on Mises material (no damage growth) and plane strain finite elements (ABAQUS). The initial stiffness in the numerical models deviates from the test result due to difficulties with accounting for different sources of local boundary flexibilities in the rig. But the FEA and line spring (LS) result correspond well in the initial part of the curve. For the 7 mm crack analyses the LS curve is somewhat gentler than the FEA curve. One reason for this is that the hardening in the line spring was modelled by a constant (average) plastic modulus whereas the plane strain element model employs the measured stress–strain curve as model for hardening behaviour. The test result shows a limit point due to the ductile crack growth. However, the numerical results in the initial plastic regime correspond quite well to the test result. One should note that the two numerical models have number of unknowns differing by four orders of magnitude.

Additional analyses were carried out for the T-connection with a 4 mm crack. The cor-

respondence between the LS and FEA curve in this case is good. One reason for the earlier nonlinear behaviour in the FEA curve compared to the LS curve is a gradually increasing crack tip plastic zone not accounted for in the line spring model. Remedies for this have been developed by Lee and Parks (1995).

Figure 6(c) shows the evolution of the J-integral obtained from the plane strain finite element model and the line spring model when $a = 7$ mm. Here correspondence is good for fully developed plastic behaviour. The plastic J-contribution from the bending and shear in the line spring are also plotted. Interestingly, one sees that the shear (Mode II) contribution is significant, and neglecting this in the line spring simulation leads to an underprediction of the computed line spring J-integral in this mixed mode situation.

2.4. Analysis of a three point bend specimen

The specimen drawn in Fig. 7(a) was tested and analysed with different planar finite element models (Rabben, 1995; Skallerud and Zhang, 1997). Figure 7(b) depicts the different load–displacement behaviour for the models along with the test result. The test result curve shows a limit point later in the displacement application. Two planar FEA model results are plotted, one assuming plane stress and one with plane strain. It is noted that the test result is located between these two curves, and a 3-D solid element model captures a more correct constraint for the plastic zone (Skallerud and Zhang, 1997). The corresponding line spring results, however, corresponds quite well with the FEA results. Also here the part of the specimen on each side of the crack were assumed rigid. Additionally, a line spring model with a modified yield stress was applied (LS curve). If we denote a yield stress constraint factor by α, we know that it should be bounded by one (plane stress) and 1.45 (plane strain, 1.15, and 1.26 due to crack). The specimen thickness requirement for a plane strain plastic zone may be written $B_I > m_{size} * \delta_{Ic}.m_{size}$ has been calculated to be in the range 25–200, depending on loading condition and specimen geometry (McMeeking and Parks, 1979). Expressing the constraint as an exponential function of the ratio of actual thickness B to required plane strain thickness B_I, the following relationship is proposed:

$$\alpha = 1 - 0.17^{1/\left(1-\frac{B}{B_I}\right)} + 0.45 \cdot e^{\left(\frac{B}{B_I}-1\right)}, \quad (B > B_I \rightarrow B = B_I) \tag{13}$$

For the actual material tested the critical CTOD is approximately 0.5 mm at room temperature. Using $m_{size} = 100$ one obtains $\alpha = 1.23$. This value is used for the LS curve in Fig. 7(b). The relationship is a pure fitting here, and needs of course more study in order to check its validity.

3. Shell and line spring finite elements

The situations analysed in the previous part correspond to the configuration illustrated in Fig. 8(a) and (b), taking the width of the crack, c, equal to plate width. Then the assumption of rigid plates connected by line springs is reasonable. For semi-elliptical cracks, however, such an assumption may be erroneous as some parts of the shell midsection are intact. These parts restrain the deformation of the cracked part of the shell. In order to account for this the plates are modelled by means of shell elements in the following. For horizontally fixed boundary conditions, shell membrane stresses develop for increasing out-of-plane displacement. The static system for the

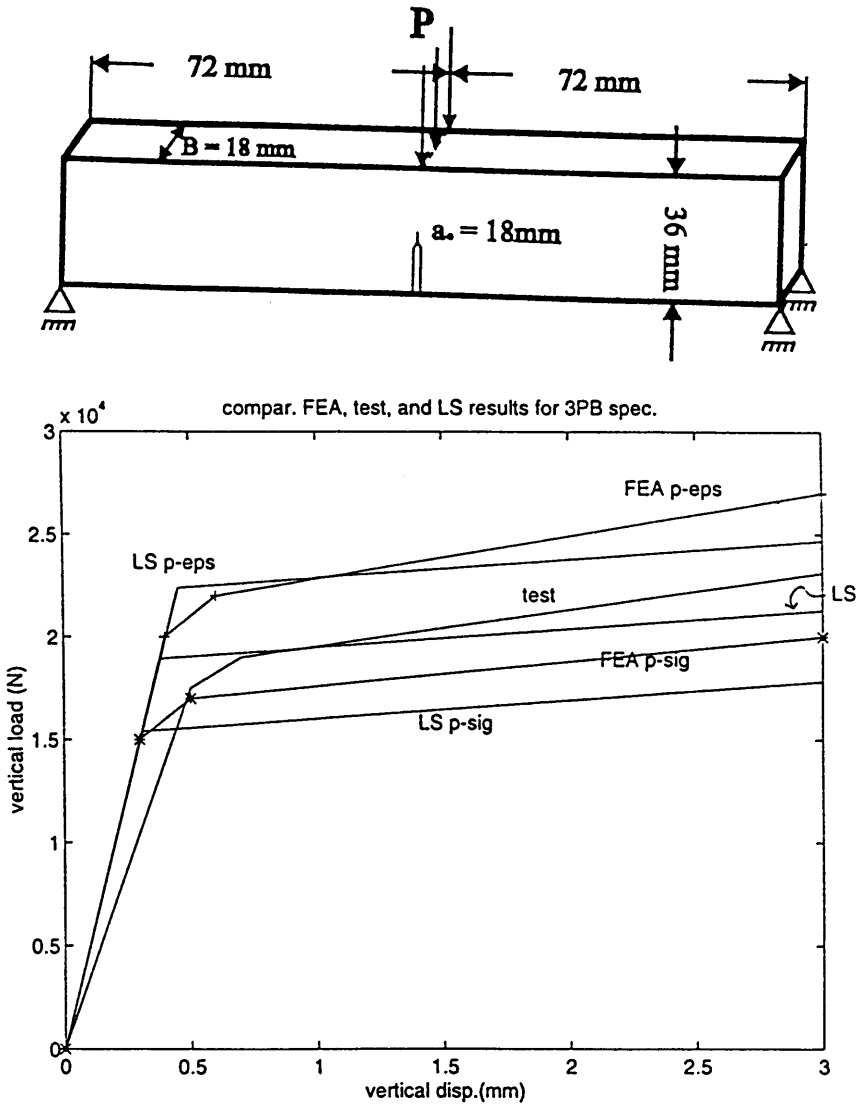

Fig. 7. (a) Three point bend specimen, (b) load vs displacement.

uncracked and cracked half-plate parts are depicted in Fig. 8(c) and (d), respectively. The system in Fig. 8(a) is analysed subsequently, both with the load applied along the center line (as shown) and by symmetric four point bending.

3.1. Finite element formulation

A total Lagrangian description of motion is employed. The stress and strain measures employed are two Piola–Kirchoff (2PK) and Green–Lagrange (GL), respectively. The reference xy-plane is

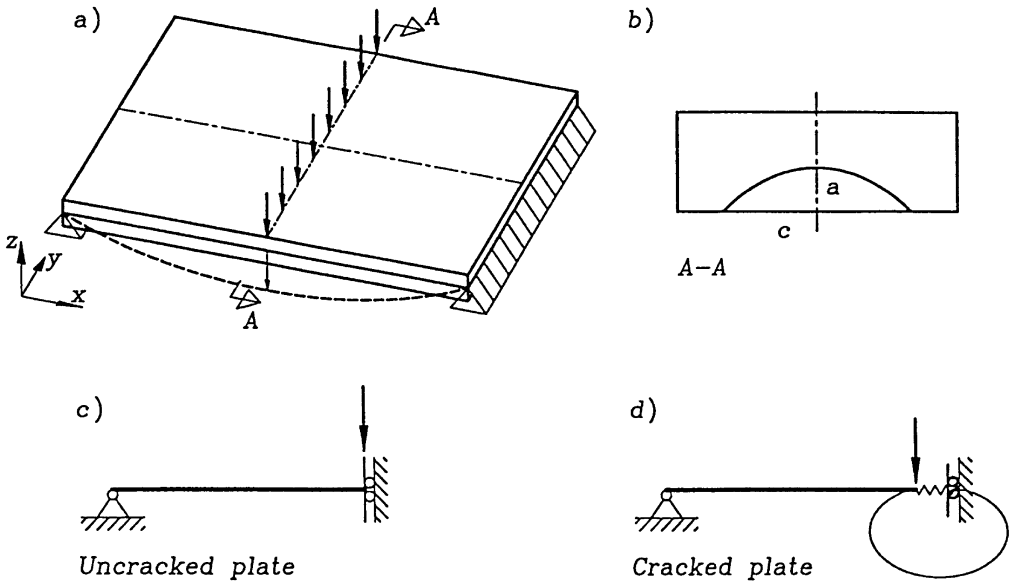

Fig. 8. Surface cracked plate.

through the mid-thickness plane of the unloaded structure. From the geometries analysed, some simplification in the strain description is utilized. The vertical displacement under the load application is restrained to be equal, and the vertical motion at the left and right boundaries is zero. Hence, the curvature of the plate in y-direction will be very small (zero at the displacement boundaries). The only nonlinear strain term accounted for in the present study stems from curvature in x-direction. Furthermore, the in-plane shear deformations will be small, especially for the case where the left and right boundaries are fixed with respect to x-displacement.

A rectangular four-node Mindlin type of shell element with 20 degrees of freedom is chosen herein, hence simulating the shear deformation in the zx- and zy-plane. The element degrees of freedom (with positive directions) are shown in Fig. 9. Denoting the bi-linear interpolation polynomials by $\mathbf{N}$ (i.e. $u = \mathbf{N}\mathbf{v}_u$ etc.) and the differentiation of $\mathbf{N}$ with respect to x and y by $\mathbf{B}_x$ and $\mathbf{B}_y$, respectively, the connection between the strain components and the nodal DOF for the situations analysed herein reads:

$$\mathbf{E} = \begin{bmatrix} E_{xx} \\ E_{yy} \\ E_{zx} \\ E_{zy} \\ E_{xy} \end{bmatrix} = \begin{bmatrix} \mathbf{B}_x & \mathbf{0} & \frac{1}{2}\mathbf{v}_w^T\mathbf{B}_x^T\mathbf{B}_x & -z\mathbf{B}_x & \mathbf{0} \\ \mathbf{0} & \mathbf{B}_y & \mathbf{0} & \mathbf{0} & -z\mathbf{B}_y \\ \mathbf{0} & \mathbf{0} & \mathbf{B}_x & -\mathbf{N} & \mathbf{0} \\ \mathbf{0} & \mathbf{0} & \mathbf{B}_y & \mathbf{0} & -\mathbf{N} \\ \mathbf{B}_y & \mathbf{B}_x & \mathbf{0} & -z\mathbf{B}_y & -z\mathbf{B}_x \end{bmatrix} \begin{bmatrix} \mathbf{v}_u \\ \mathbf{v}_v \\ \mathbf{v}_w \\ \mathbf{v}_{\theta y} \\ \mathbf{v}_{\theta x} \end{bmatrix} = \left(\mathbf{B}_L + \tfrac{1}{2}\mathbf{B}_{NL}\right)\mathbf{v} \tag{14}$$

$\mathbf{v}_{u,v,w,\theta y,\theta x}$ are the $5 \times (4 \times 1)$ column matrix with DOF corresponding to x, y, z displacements and rotations about the y- and x-axis, respectively. Note that the only nonzero contribution to $\mathbf{B}_{NL}$ is

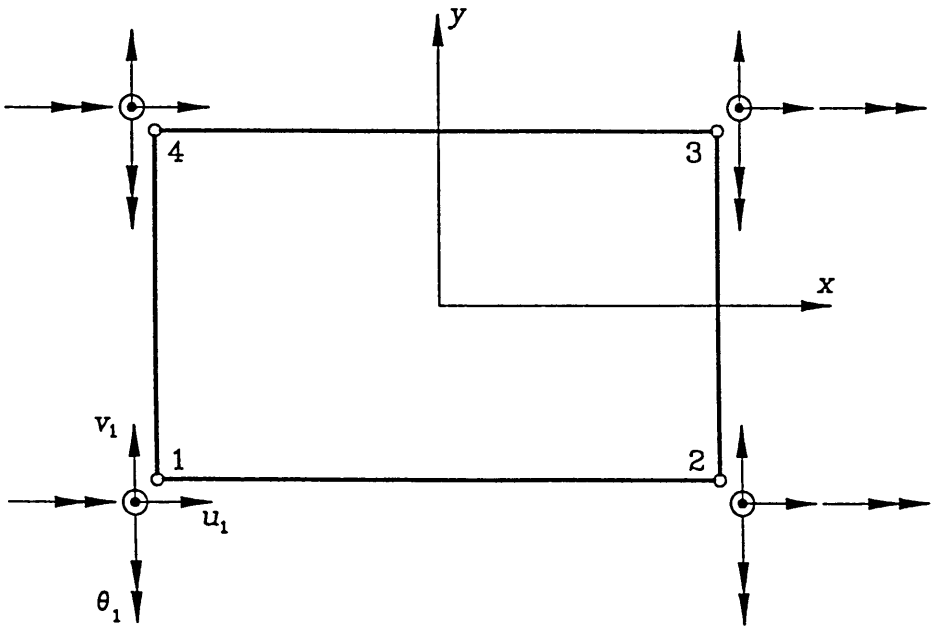

Fig. 9. Shell finite element.

the term $\mathbf{v}_w^T\mathbf{B}_x^T\mathbf{B}_x$, linking the out-of-plane displacement to the axial stress, i.e. a von Karman linearisation in the x-direction.

The incremental relationship between the 2PK stresses and GL strains is expressed in the usual way:

$$\mathrm{d}\mathbf{S} = \left[\mathbf{D}_e - \frac{\left(\mathbf{D}_e \dfrac{\partial f}{\partial \mathbf{S}}\right)\left(\mathbf{D}_e \dfrac{\partial f}{\partial \mathbf{S}}\right)^T}{\dfrac{\partial f^T}{\partial \mathbf{S}} \mathbf{D}_e \dfrac{\partial f}{\partial \mathbf{S}} + E_p} \right] \mathrm{d}\mathbf{E} = \mathbf{D}\,\mathrm{d}\mathbf{E} \tag{15}$$

Here $\mathbf{D}_e$ is the elasticity matrix for the material, E_p is the hardening. The shell material is assumed to follow a linear isotropic hardening rule, and the von Mises yield surface is employed in the above equation.

The discretized expression for the weak form of incremental equilibrium is obtained from the incremental virtual displacement principle, and reads:

$$\int_{V_{\text{elem}}} [\delta\mathbf{v}^T(\mathbf{B}_L + \mathbf{B}_{NL})^T\mathbf{D}(\mathbf{B}_L + \mathbf{B}_{NL})\Delta\mathbf{v} + S_{xx}\delta\Delta\mathbf{E}]\,\mathrm{d}V_{\text{elem}} = \delta\mathbf{v}^T\Delta\mathbf{R}_{\text{ext,elem}} \tag{16}$$

$$\Rightarrow \mathbf{k}_{\text{elem}}\Delta\mathbf{v} = \Delta\mathbf{R}_{\text{ext,elem}}$$

The term with S_{xx}, initial stress stiffness, accounts for the increasing membrane action for increasing out-of-plane displacements. $\mathbf{R}_{\text{ext,elem}}$ is the element nodal forces due to external loads. The in-plane

integration of the element is carried out by means of a 2×2 Gauss quadrature for all terms. This full integration causes problems with shear locking for thin shell elements, but in the simulations below, the shell elements do not have such small thickness to length ratios. The integration over the shell thickness is carried out by the five point Lobatto rule, hence capturing extreme fiber first yield in bending. The linearly interpolated line spring element is integrated with a one point Gauss rule.

The above relationships were implemented and run with MATLAB syntax. All equations are solved by the explicit Euler method, keeping increments sufficiently small in order to prevent significant drift from the correct solution.

3.2. Analysis of an intact plate

In order to check the shell element performance, the geometry shown in Fig. 8(a) was analysed with SHEL*ls*. One quarter of the plate was modelled with 16 shell elements (4×4). The left and right edges were fixed with respect to x-displacement in order to develop membrane stresses. The material was taken to be nonhardening, hence having the opportunity to compare with the rigid plastic solution given in eqn (12). The thickness to half-length for the plate was 0.19. Figure 10 shows the transversal load vs transversal displacement for the simulation and the analytic solution. The initial bending dominated, load carrying capacity is overpredicted somewhat. This is explained by the relatively coarse FE mesh and using five integration points through thickness. For increasing deflections, however, the simulation merges quite well with the analytic solution, indicating that the membrane action is appropriately accounted for. One should note that the stress history in some of the inelastic integration points is very non-proportional, e.g. the upper surface stress goes from compressive to tensile as the membrane force takes over the load carrying.

3.3. Analysis of a cracked plate in four point bending without membrane action

White *et al.* (1983) have reported test results for cracked wide plates loaded in four point bending. One of their tests, denoted SC18 in the reference, was analysed herein with 4×4 shell elements and two line spring elements (length 10 and 2.7 mm) for 1/4 of the plate. The crack in the test specimen is semi-elliptical with $a/t = a/c = 0.35$. The material has yield strength 496 MPa, and is low-hardening. In the simulations it is assumed a constant plastic modulus of magnitude 1780 MPa. Note that the ratio of crack width to plate width, c/b, is quite small, 0.25. Hence, the crack area is small compared to remaining shell area. Figure 11(a) illustrates the load vs crack mouth opening displacement curves for the test and simulation. The CMOD is measured slightly above the specimen surface, therefore it is denoted modified CMOD in the figure. Some over-prediction in stiffness is observed in the elastic plastic transition, but in the fully plastic regime, the simulation corresponds quite well with the test. It should be noted that White *et al.* (1983) also simulated this test with a finer element mesh (28 plate and four line spring elements), and with seven Lobatto points through thickness. This simulation follows the test result nicely, although the initial elastic stiffness is somewhat overpredicted.

Figure 11(b) illustrates the evolution of the J-integral in the SHEL*ls* simulation. The integration points for the two line spring elements correspond to the parametric angles ϕ equal 1.1 and 0.47 radians, respectively. These angles are measured on a circular arc going from the surface of the

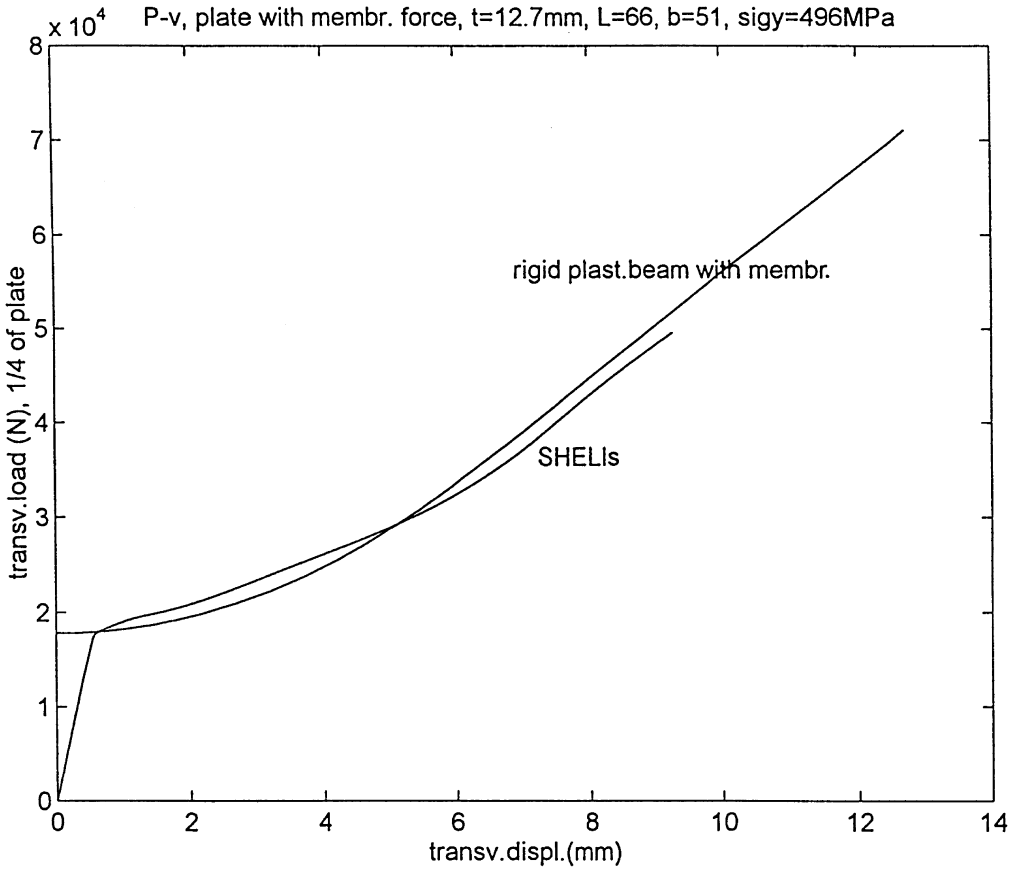

Fig. 10. Load vs displacement for intact plate with membrane force.

specimen to the deepest point of the crack. The J-integral prediction is underestimated somewhat when compared to the line spring calculation of J obtained by White *et al.* (1983). For the line spring calculation representing the central part of the crack, where the crack front curvature is small, the correspondence between the two simulations is improving for increasing deformation. As accurate J-predictions requires a finer mesh, and is not a main goal in the present study, the results are considered acceptable for the subsequent simulations. Note that in the present simulations, if the net incremental crack tip opening contribution according to eqn (9) is less than zero, the J-increment is set to zero.

3.4. Analysis of cracked shells with membrane action

The four point bend specimen described in the previous section is now modified to have horizontally restrained x-displacements at the left and right boundary, see also Fig. 2. The yield stress and plastic modulus are the same as above. In the simulations shown in Fig. 12(a), one accounts and one does not account for the initial stress term. The significant load increase due to

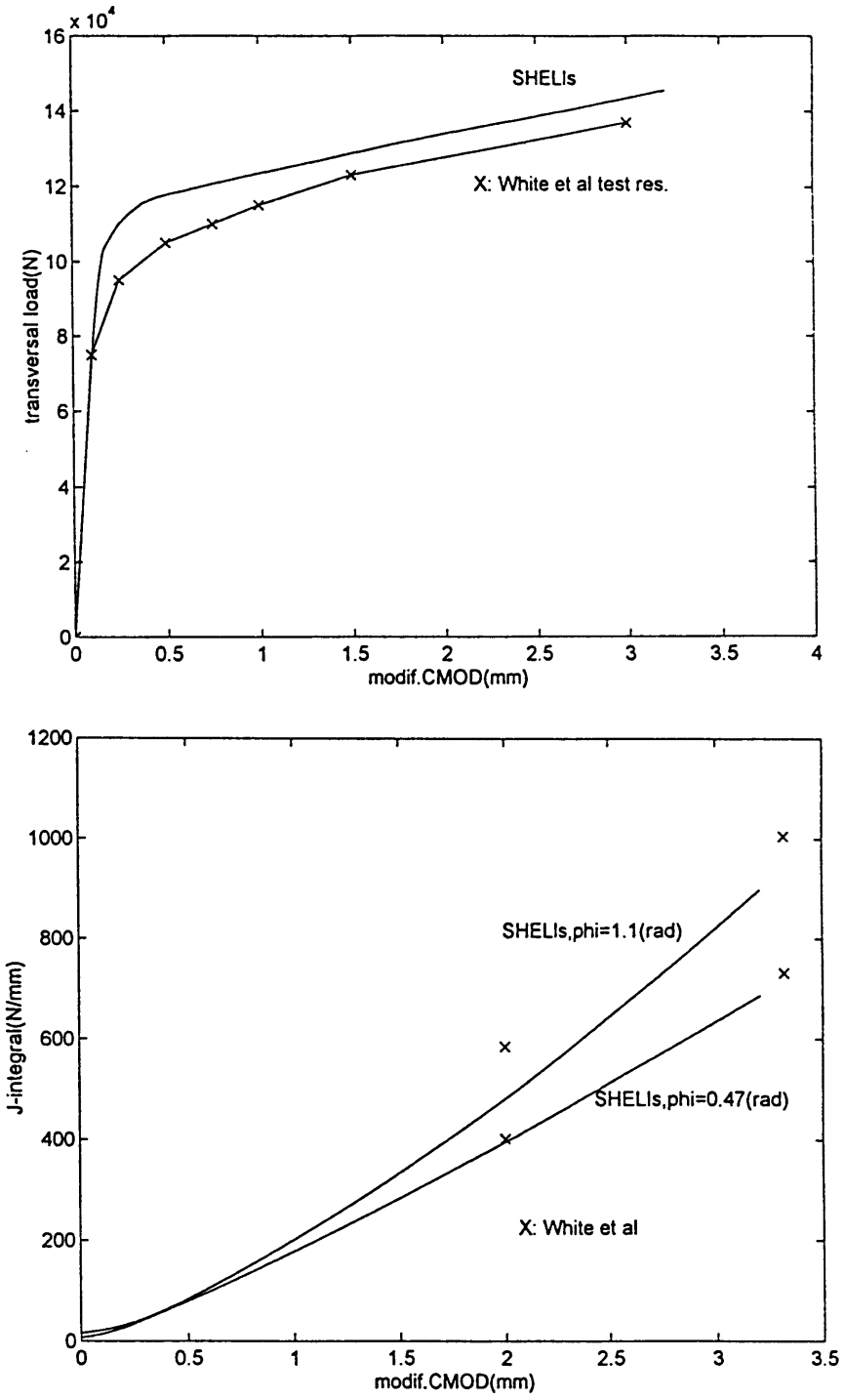

Fig. 11. (a) Load vs CMOD for cracked plate without membrane force, (b) corresponding J-integral evolution.

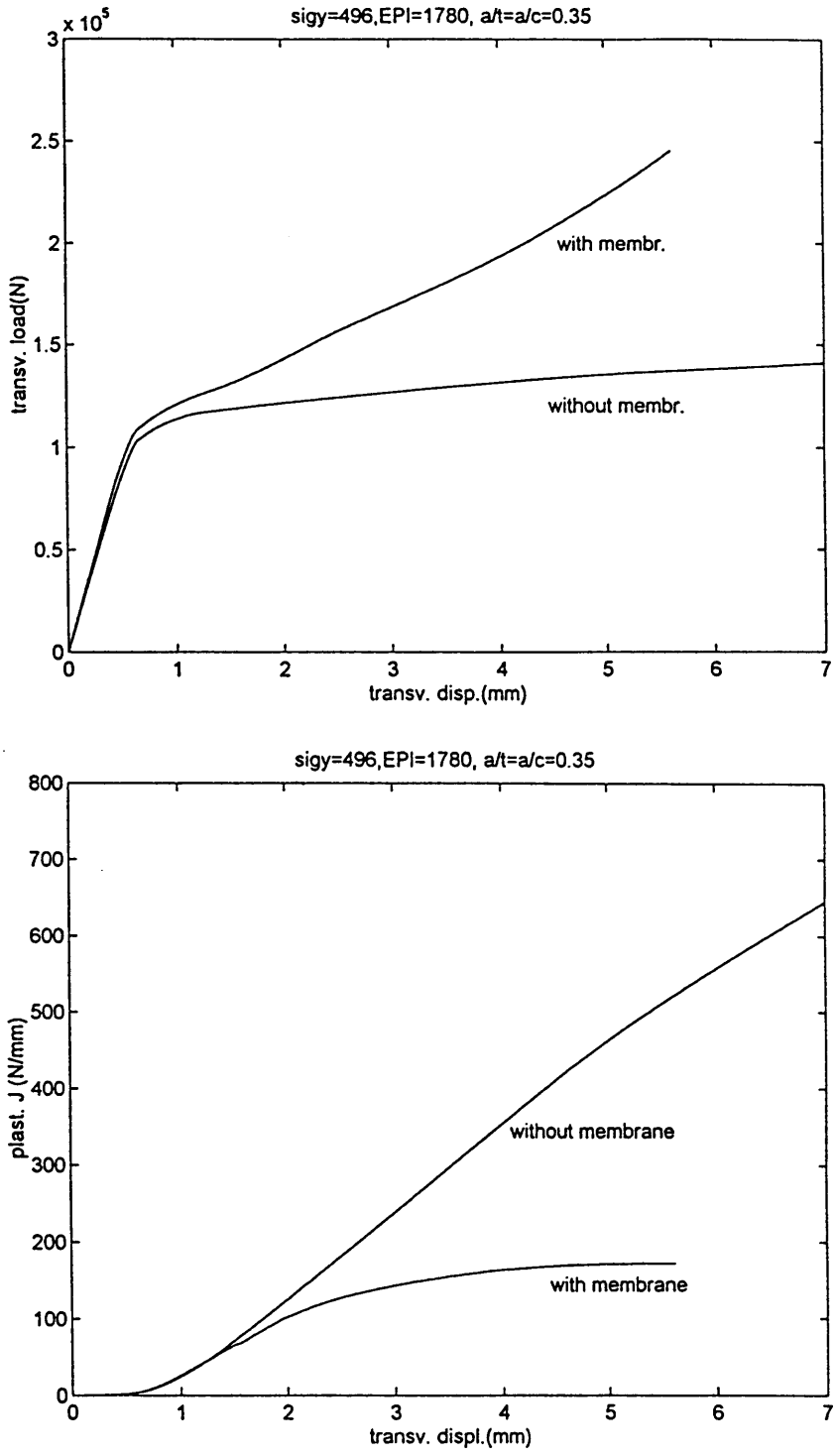

Fig. 12. (a) Load vs displacement, (b) plastic J-integral, (c) line spring deformation.

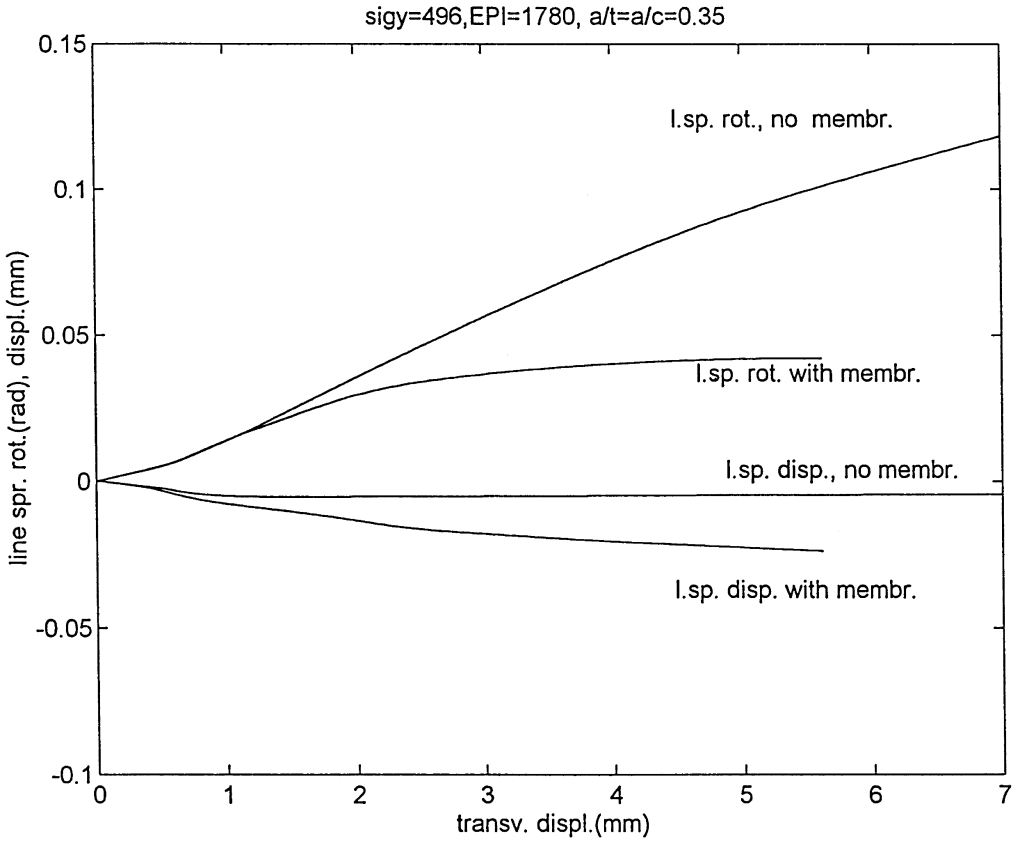

Fig. 12—*Continued.*

the membrane action is clearly seen. Nothing new is exhibited in this plot compared to the plots in Part 1, but turning to Fig. 12(b) one observes that the J-integral for the integration point in the central line spring element saturates to a constant value (for the displacement level plotted) when membrane force is accounted for. If the plate carries load in bending only, this saturation is much slower. The explanation for this behaviour is the fact that the redistribution of load to the intact parts of the shell is more significant if membrane stresses contributes to load carrying. The intact parts of the shell constrains the cracked section both with respect to in-plane deformations and rotations, and depending on whether the load is carried by bending only, these constraints affect the line spring deformations differently. Note also that assuming rigid plate-inelastic line spring as in Part 1, the line spring rotation follows $\theta = \arcsin(v/l)$ or $\arctan(v/l)$ for horizontally unrestrained or fixed x-motion, respectively, i.e. the two cases have an increasing or decreasing rotation evolution. This is further illustrated in Fig. 12(c) where the line spring integration point rotation and extension are plotted. The negative part of the ordinate axis gives the extension, the positive part the rotation. One observes that if the load is carried by bending only, the rotation is much larger than the corresponding simulation with membrane action. The extension is approximately zero for the bending only simulation, whereas the membrane action leads to a somewhat larger

extension of the line spring. These deformations do saturate in the simulation with membrane action, and according to the calculation of the J-integral, decreasing line spring deformation increments leads to decreasing crack tip displacement increments. Hence, the J-integral saturates due to the significant restraint from the intact part of the shell.

In order to investigate the effect of the crack width on the cracked shell behaviour, an additional analysis was run with $c/b = 0.8$ (in the previous example $c/b = 0.25$). Figure 13(a) shows several load–displacement curves. Curves that may be compared are the two accounting for membrane forces, they are based on similar a/t ratios and elastic–perfectly plastic material. The abscissa axis is transversal displacement normalized with the distance between the load application and the boundary. Corresponding J-integral evolution is plotted in Fig. 13(b). The saturation of J observed for the plate with the smallest crack is not occurring to the same extent for the wider crack. It exhibits a competition between increase and saturation, governed by the evolution of line spring deformations and load redistribution to the intact parts of the shell. The curve representing the plate without membrane action is located between the two curves accounting for membrane action for the displacement level shown.

Other a/t- and a/c-ratios show similar behaviour as illustrated by Fig. 13. Increasing the crack depth yields a line spring that needs larger transversal displacement in order to reach a full membrane load condition. If the structural configuration is according to three point bending, a similar delayed membrane evolution is observed. An important difference between the four and three point bending systems is that the four point bend has a larger membrane force effect, as the part of the plate between the load application points tends to straighten. This does not occur in three point bending.

4. Concluding remarks

The present investigation has addressed the effects of second order membrane effects on the response of cracked shells loaded out-of-plane. The main objective was to investigate qualitatively the response of shells subjected to finite out-of-plane displacements. In order to isolate effects, some simplified components were analysed first, assuming rigid cracked plates connected by elastic–plastic line springs. This represents plates with crack-width equal to plate width. It is noted that in components with restraints against in-plane deformation subjected to finite out-of-plane deformations, the membrane contribution to the J-integral is significant, and is the main contribution for transversal deflections larger than approximately two times the ligament size. Assuming pure bending as load carrying in such situations, the J-integral will be underestimated significantly if the load is applied in displacement control. An eccentrically cracked plate was also analysed with the simplified approach. This example contains both Mode I and II crack deformations. The line spring model corresponds well with both detailed plane strain FEA results and test results. The importance of being able to calculate the Mode II J-contribution is pointed out.

Turning to surface cracks of finite width, shell and line spring finite element analyses of cracked plates in four point bending were carried out. Now the crack width to plate width ratio becomes an important parameter due to the significant capability of the shell to redistribute load to the intact part of the shell. In a displacement controlled load situation, assuming vanishing restraint

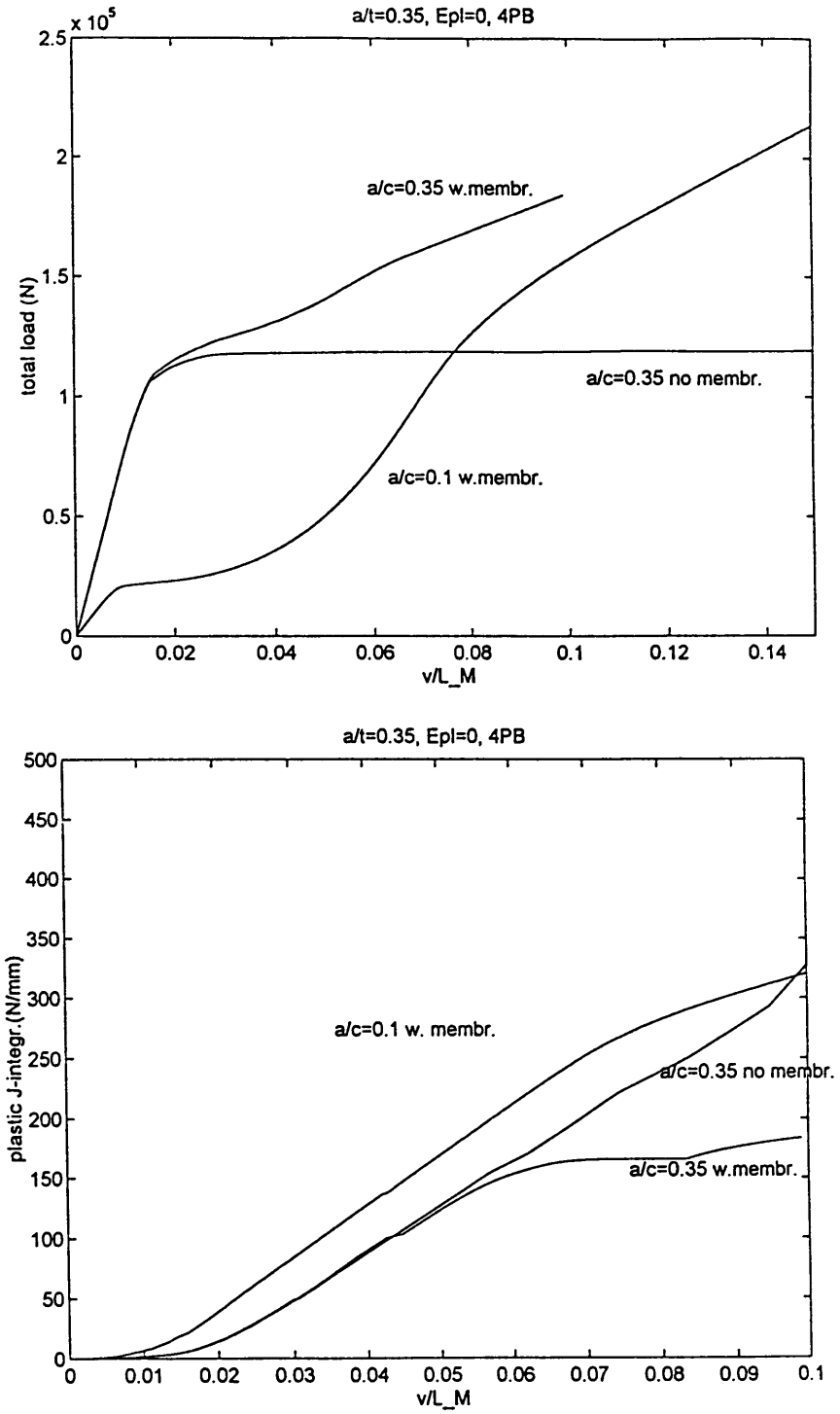

Fig. 13. Effects of crack width: (a) load vs displacement, (b) plastic J-integral, (c) line spring deformation.

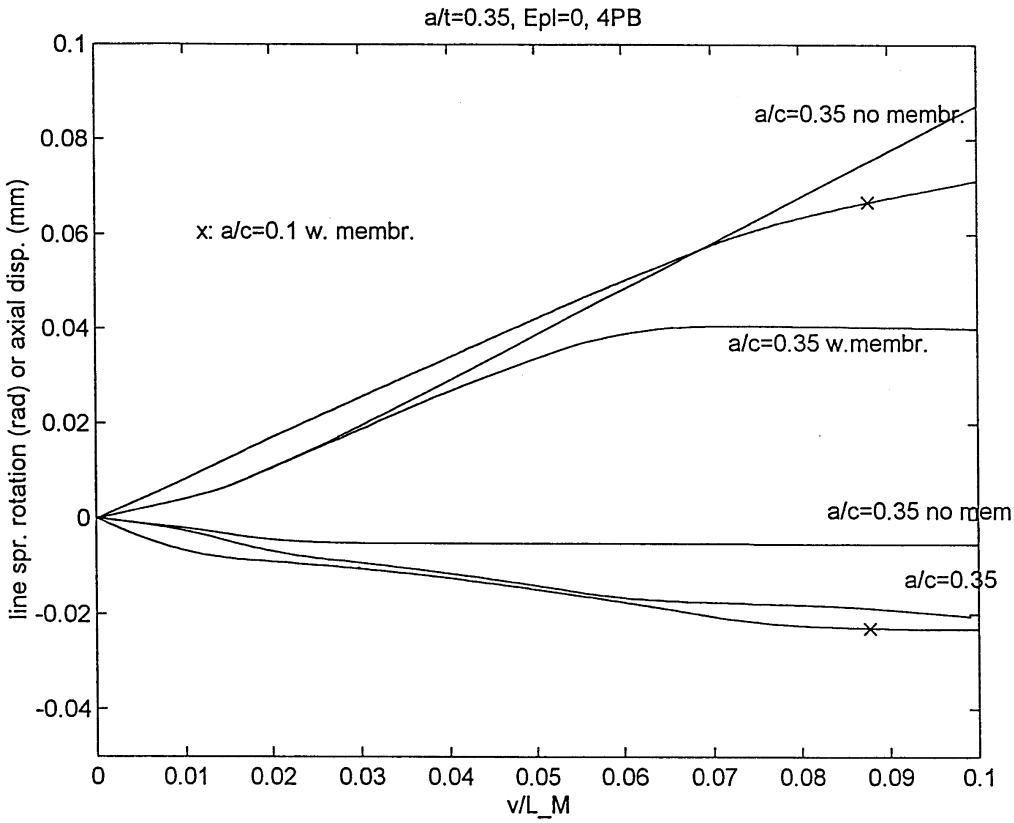

Fig. 13—*Continued.*

against in-plane (axial) deformations leads to conservative J-predictions. Hence, it is not obvious to state whether accounting for the membrane action in a fracture mechanical assessment of a semi-elliptically cracked shell is conservative. The number of parameters that affect this result increases compared to analyses assuming linear geometry (small displacement gradients). In conclusion the following parameters should be considered in a total assessment of the capacity of a cracked shell: a/t, a/c, c/b, v/t, load or displacement control of external actions, stress–strain curve, crack growth initiation parameter J_c, δ_c, in-plane restraints, and constraint (T, Q, or m).

In further investigations of the problems addressed herein, other geometries and load conditions should be analysed. In the present study no actual fracture assessment has been performed, only response and J-integral evolution have been presented. Hence, a synthesis of analysis (shell and line spring finite elements, linear/nonlinear geometry), J-calculation, and fracture initiation prediction should be carried out, and compared with corresponding test results. Furthermore, the capability of the line spring to simulate ductile tearing in the above finite element setting should be studied.

References

Betegon, C. and Hancock, J. W. (1991) Two-parameter characterization of elastic plastic crack-tip fields. *Journal of Applied Mechanics* **58,** 104–110.

Cottrell, A. H. (1961) Theoretical aspects of radiation damage and brittle fracture in steel pressure vessels. *Iron Steel Inst. Spec. Rep. No.* 69, pp. 281–296.

Crisfield, M. A. (1997) *Nonlinear Analysis of Solids and Structures*, Vol. 2. John Wiley.

Kirk, M. and Bakker, A. (1995) Constraint effects in fracture and application, Vol. 2. *ASTM STP* 1244, Philadelphia.

Lee, H. and Parks, D. M. (1993) Fully plastic analyses of plane strain single edge cracked specimens subject to combined tension and bending. *International Journal of Fracture* **63,** 329–349.

Lee, H. and Parks, D. M. (1995) Enhanced elastic–plastic line spring finite element. *International Journal of Solids and Structures* **32,** 2393–2418.

Lee, H. and Parks, D. M. (1997) Ductile tearing line spring. *International Journal of Solids and Structures*, to appear.

McMeeking, R. M. and Parks, D. M. (1979) On criteria for *J*-dominance of crack tip in large scale yielding. *ASTM STP* 668, ed. Landes, Begley, and Clarke, pp. 175–194.

O'Dowd, N. P. and Shih, C. F. (1992) Family of crack-tip fields characterized by a triaxiality parameter—II. Fracture applications. *Journal of the Mechanics and Physics of Solids* **40,** 989–1016.

Parks, D. M. (1992) Advances in characterization of elastic–plastic crack tip fields. In: *Topics in fracture and fatigue*. ed. A. S. Argon. Springer Verlag.

Parks, D. M. and White, C. S. (1982) Elastic–plastic line spring finite elements for surface cracked plates and shells. *J. Press. Vessels Tech.* **104,** 287–292.

Rabben, D. (1996) Nonlinear analysis of ductile fracture in welded *T*-connections using micromechanical damage modelling. M.Sc. thesis, Dep. Marine Struct. NTNU, Trondheim, Norway.

Rice, J. (1968) A path independent integral and the approximate analysis of strain concentration by notches and cracks. *Journal of Applied Mechanics* **35,** 379–386.

Rice, J. and Levy, N. (1972) The part through surface crack in an elastic plate. *Journal of Applied Mechanics*, pp. 185–194.

Shih, C. F. and German, M. D. (1981) Requirements for a one-parameter characterization of crack tip fields by the HRR singularity. *International Journal of Fracture* **17,** 27–43.

Skallerud, B. (1995) Inelastic line springs in nonlinear analysis of cracked tubular joints. *Fatigue Fract. Engng Mater. Struct.* **18,** 463–477.

Skallerud, B. (1996) A mixed mode I/II inelastic line spring. *International Journal of Solids and Structures* **33,** 4143–4166.

Skallerud, B. and Zhang, Z. L. (1997) Effects of finite element mesh on the numerical prediction of ductile tearing. ASTM 29. Symp. Fatigue and Fracture, Stanford.

Skallerud, B., Rabben, D. and Zhang, Z. L. (1997) Numerical simulation of ductile tearing, in preparation.

Wells, A. A. (1961) Unstable crack propagation in metals: cleavage and fast fracture. *Proc. Crack Prop. Symp.*, Vol. 1, pp. 210–230, Cranfield.

White, C. S., Ritchie, R. O. and Parks, D. M. (1983) Ductile growth of part-through surface cracks: Experiment and analysis. *ASTM STP* 803, ed. C. F. Shih and J. P. Gudas, I384–I409.